JGR Oceans

RESEARCH ARTICLE
10.1029/2019JC015422

Special Section:
The Arctic: An AGU Joint Special Collection

Monthly Variability in Bering Strait Oceanic Volume and Heat Transports, Links to Atmospheric Circulation and Ocean Temperature, and Implications for Sea Ice Conditions

Mark C. Serreze[1], Andrew P. Barrett[1], Alex D. Crawford[2], and Rebecca A. Woodgate[3]

[1]National Snow and Ice Data Center, Cooperative Institute for Research in Environmental Sciences, University of Colorado Boulder, Boulder, CO, USA, [2]Department of Earth Sciences, College of Wooster, Wooster, OH, USA, [3]Applied Physics Laboratory, University of Washington, Seattle, WA, USA

Abstract The Bering Strait oceanic heat transport influences seasonal sea ice retreat and advance in the Chukchi Sea. Monitored since 1990, it depends on water temperature and factors controlling the volume transport, assumed to be local winds in the strait and an oceanic pressure difference between the Pacific and Arctic oceans (the "pressure head"). Recent work suggests that variability in the pressure head, especially during summer, relates to the strength of the zonal wind in the East Siberian Sea that raises or drops sea surface height in this area via Ekman transport. We confirm that westward winds in the East Siberian Sea relate to a broader central Arctic pattern of high sea level pressure and note that anticyclonic winds over the central Arctic Ocean also favor low September sea ice extent for the Arctic as a whole by promoting ice convergence and positive temperature anomalies. Month-to-month persistence in the volume transport and atmospheric circulation patterns is low, but the period 1980–2017 had a significant summertime (June–August) trend toward higher sea level pressure over the central Arctic Ocean, favoring increased transports. Some recent large heat transports are associated with high water temperatures, consistent with persistence of open water in the Chukchi Sea into winter and early ice retreat in spring. The highest heat transport recorded, October 2016, resulted from high water temperatures and ideal wind conditions yielding a record-high volume transport. November and December 2005, the only months with southward volume (and thus heat) transports, were associated with southward winds in the strait.

Plain Language Summary The Chukchi Sea is a focus of resource exploration, and all vessels transiting the Arctic Ocean must pass through it. Sea ice conditions that affect operations in this area are influenced by month-to-month variations in how much oceanic heat is brought into the region from the Pacific Ocean via the Bering Strait, the narrow (~85 km wide) channel separating Russia (Chukotka) from the United States (Alaska). The oceanic heat transport depends on both the temperature of the water and volume of water that is transported. The volume transport is in part controlled by surface winds in the strait and along the East Siberian Sea coast. We show that the latter are part of a larger pattern of atmospheric circulation influencing September sea ice extent for the Arctic Ocean as a whole. We use case studies for individual months to document the varying roles on the oceanic heat transport played by water temperature, winds in the East Siberian Sea, and local winds in the Bering Strait.

Key Points:
- Central Arctic anticyclonic winds favor low September sea ice extent by promoting convergence, warm conditions, and a large oceanic heat flux through Bering Strait
- Summertime trends toward higher Arctic Ocean sea level pressure favored increased oceanic heat transports through the Bering Strait from 1980 to 2017
- Recent large Bering Strait heat transports coincide with high water temperatures, consistent with early ice retreat and late ice advance in the Chukchi Sea

Supporting Information:
- Supporting Information S1

Correspondence to:
M. C. Serreze,
serreze@nsidc.org

Citation:
Serreze, M. C., Barrett, A. P., Crawford, A. D., & Woodgate, R. A. (2019). Monthly variability in Bering Strait oceanic volume and heat transports, links to atmospheric circulation and ocean temperature, and implications for sea ice conditions. *Journal of Geophysical Research: Oceans*, *124*, 9317–9337. https://doi.org/10.1029/2019JC015422

Received 26 JUN 2019
Accepted 5 NOV 2019
Accepted article online 11 NOV 2019
Published online 18 DEC 2019

1. Introduction

As the Arctic Ocean loses its summer sea ice cover and the winter ice cover thins, it becomes increasingly accessible for oil and natural gas exploration and development, marine transport, tourism, and other activities (U.S. Navy, 2014). In recognition of this, there is growing interest in improved predictions of sea ice retreat dates, open water duration, and ice advance dates, especially at seasonal lead times on the regional spatial scales most relevant to supporting economic activities (Serreze & Meier, 2018). The Chukchi Sea stands out in this regard (Figure 1). This shallow sea is a focus of resource exploration, and all vessels transiting the Arctic Ocean must pass through it.

The Chukchi Sea is linked to the North Pacific Ocean via inflow of comparatively (to the Arctic) fresh waters, warm in summer and cold in winter, through the Bering Strait. This shallow (50 m) and narrow (85 km) strait is split roughly in the middle by two islands—Big and Little Diomede (Woodgate et al., 2015).

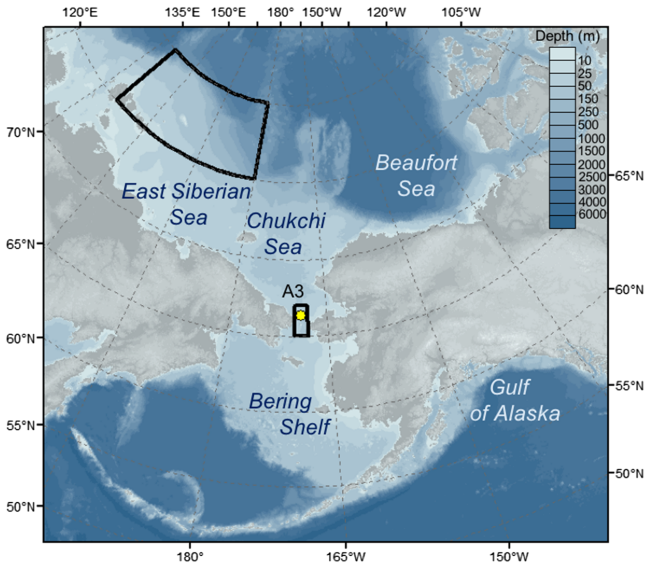

Figure 1. The study region, showing bathymetry, the location of the A3 mooring (yellow dot), and the areas (black-framed regions) where 10-m winds are assessed in the East Siberian Sea and the Bering Strait (see text).

Volume transport, water temperature, and salinity in the strait have been measured since 1990 via mooring arrays (Woodgate, 2018). The volume inflow has long been assumed as driven by an oceanic pressure difference between the North Pacific and Arctic Oceans (the "pressure head"), whose influence is strongly modified by local winds in the strait (e.g., Coachman & Aagaard, 1966; see Woodgate et al., 2005a, 2015, and Woodgate, 2018, for discussion).

The oceanic heat carried by waters entering through the Bering Strait (the Bering Strait "heat transport") is implicated in the seasonal melt back of sea ice in the Chukchi Sea region (Fedorova & Yankina, 1963; Paquette & Bourke, 1974; Ahlnas & Garrison, 1985; Spall, 2007; Woodgate et al., 2010; Woodgate et al., 2015; Serreze et al., 2016a). Woodgate et al. (2010) argue that, along with acting as a trigger for the onset of the seasonal melt back in the Chukchi Sea, the inflow may provide a subsurface heat reservoir for much of the western Arctic Ocean, influencing ice extent/thickness over that region. Their study speculated on the relationship between the large annual inflow recorded for 2007 (~5.3×10^{20} J, relative to −1.9 °C) and the (then) record low September ice extent for the Arctic as a whole. Continuing this theme, Serreze et al. (2016) show that two thirds of the variance in the retreat date of sea ice in the Chukchi Sea can be explained by the Bering Strait heat inflow averaged from April to June. They also showed that about two thirds of the variance in the date of seasonal ice advance can similarly be explained by the combined influences of the Bering Strait heat transport averaged from July to September and the date of ice retreat in the spring of the same year. The link with the retreat date likely depends also on local seasonal ocean heat uptake. An earlier retreat leads to more oceanic heat gain in the Chukchi Sea through spring, meaning that more heat must be lost in autumn before ice can form. The Bering Strait mooring data document upward trends since 1990 in both the annually averaged volume and heat transports, the latter largely driven by the changing volume transport (Woodgate, 2018), accompanied by a modest warming.

Motivated by identified links with sea ice conditions, the present paper aims to clarify the complex interplays between the heat transport, the volume transport, water temperatures, and atmospheric circulation patterns. Previous authors (Peralta-Ferriz & Woodgate, 2017) have suggested that zonal wind anomalies in the East Siberian Sea play a key role in the monthly variability of the volume (hence heat) transport through the strait. We confirm these are regional expressions of a well-known tendency for the large-scale atmospheric circulation over the central Arctic Ocean to vary between anticyclonic and cyclonic conditions. We show that this links the Bering Strait volume (and heat) transport to processes known to influence end-of-summer sea ice extent for the Arctic Ocean as a whole. We use a series of case studies to highlight how different combinations of zonal winds in the East Siberian Sea, meridional winds in the Bering Strait, and water temperatures in the strait can combine to yield a very large northward heat transport (e.g., October 2016) or a small or even southward heat transport (November and December 2005).

2. Overview of the Bering Strait Transport

The Bering Strait transport to the Arctic has two basic components. The largest component of the transport is a generally northward flow through both channels of the strait, seasonally warm and cold, highly correlated with the local winds (so flow reversals are common under strong southward winds), and order 1 Sv in the annual mean (see Woodgate, 2018; Woodgate et al., 2015). This flow component has been measured year-round by in situ moorings since 1990. The second component is a seasonally present warm, fresh coastal current, the Alaskan Coastal Current (ACC), present along the U.S. coast from summer to winter, and order 0.1 Sv in the annual mean (Woodgate et al., 2006; see Woodgate, 2018) for discussion. This component has only been measured since 2001.

Both components reflect local wind forcing and, although northward in the annual mean, may reverse on time scales of days in response to strong southward winds. The ACC, seasonal ice melt, and heating are

likely the primary drivers of the seasonally present two-layer system (approximately) in the Bering Strait and Chukchi Sea water column (Woodgate et al., 2015). The upper layer, which is fresher (and typically warmer), is about 10–20 m thick and is found during summer to late autumn, while the lower layer tends to be saltier and usually colder (Woodgate et al., 2005a; Woodgate et al., 2012; 2015). The ACC is typically present from late April to December (Woodgate & Aagaard, 2005). Its freshness and warmth suggest a strong influence of river input, especially from the Yukon, other Alaskan rivers, and the Gulf of Alaska (Aagaard et al., 2006; Morris, 2019). While under northward wind conditions the ACC is a narrow (10–20 km wide) feature, southward winds cause the ACC to separate from the Alaskan Coast, transporting warm, fresh waters into the central Chukchi Sea (Morris, 2019; Woodgate et al., 2015). Although the volume transport associated with the ACC is ~10% of the total volume transport, it is estimated to carry about a third of the heat and about a quarter of the total freshwater flux (Woodgate et al., 2006; Woodgate et al., 2015; Woodgate, 2018), relative to −1.9 °C and 34.8 psu, respectively. The ACC should not be confused with the very similarly named Alaska (no letter n) Coastal Current found in the Gulf of Alaska.

As in previous studies, we use heat fluxes calculated by

$$T_{\mathrm{Heat}} = \rho T_{\mathrm{vol}} C_{\mathrm{w}} \left(\Theta - \Theta_{\mathrm{ref}}\right),$$

where T_{Heat} is the heat transport, ρ is the density of seawater (1,023 kg/m^3), T_{vol} is the volume transport through the strait, C_{w} is the specific heat capacity of water (3,900 J·kg^{-1}·K^{-1}), is the water temperature, and $_{\mathrm{ref}}$ is the reference temperature (−1.9 °C), approximately the freezing point of water of Bering Strait salinities. Since Pacific waters are known to exit the Arctic at about the freezing point (Steele et al., 2004), our heat flux is then the amount of heat lost from Pacific waters during their time in the Arctic (Woodgate et al., 2010).

Thus calculated, the heat transport through the Bering Strait has a minimum in winter (when the water is near its salinity-adjusted freezing point) and maxima typically in August or September, but as early as June and as late at October (Woodgate, 2018; Woodgate et al., 2010). The seasonal maximum is driven by both the higher water temperatures in summer and a general summer maximum in the volume transport (Woodgate et al., 2005b). Woodgate (2018) find significant interannual trends in the volume and heat fluxes and significant warming trends in temperature in some of the summer months. The warming trends link to an earlier arrival of warm waters in the strait. Woodgate (2018) conclude that the volume flux increase is primarily due to change in the pressure head.

The interplay of factors driving the volume transport through the strait and its variability, hence bearing on the heat transport, has been an issue of long-standing debate—see discussions in Woodgate (2018) and Peralta-Ferriz and Woodgate (2017). The old traditional view was one of a fairly constant pressure head driving a northward flow, which was then modulated by the local winds in the strait, which are (especially in winter) generally southward, opposing the mean northward inflow (Coachman & Aagaard, 1966). Indeed, the role of local winds in the strait has repeatedly been recognized as influencing short-term variability (with anomalous northward blowing winds promoting a stronger northward volume transport; see Woodgate et al., 2005b). However, the origin of the pressure head and its variability has been less clear.

Previous work argued that the pressure head is steric in origin (Aagaard et al., 2006; Stigebrandt, 1984) associated with relatively low salinities (hence low density) in the North Pacific. More recent work however relates the pressure head forcing instead to winds primarily in the Bering Shelf region (Danielson, Hedstrom, et al., 2012; Danielson, Weingartner, et al., 2012). In particular, Danielson et al. (2014) developed a conceptual model that linked the Bering Strait volume transport variability to the longitudinal location of the atmospheric Aleutian Low and used a simple barotropic model, which suggests winds over the Bering Shelf have a much greater (2–3 times) influence on the Bering Strait variability than winds within the Arctic. Thus, their study focuses on the Pacific influence, although they also discuss drivings from winds over the East Siberian Sea and conclude they are small. However, it should be noted that their barotropic model significantly (by a factor of 2) underestimates the observed variance at A3 and thus may have important differences to the real-world system.

Peralta-Ferriz and Woodgate (2017), considering a somewhat different time period, 2002–2016, compared to Danielson et al.'s 1997 to 2011 focus, took a new look at the problem using an empirical orthogonal function (EOF) analysis of the available gridded time series of ocean bottom pressure anomalies from the NASA

GRACE satellite (Save et al., 2016). They assessed relationships between time series of the first two EOF modes (the principal components [PCs] of the modes) of ocean bottom pressure and variability in the monthly time series of the Bering Strait volume transport. They examined both the total volume transport and an estimate of the pressure head-driven portion of the transport (the portion not correlated with the local winds), relating them to ocean bottom pressure, surface winds, and sea level pressure (SLP) patterns in the Bering and Arctic regions.

In contrast to Danielson et al. (2014), they present strong evidence that processes in the Arctic Ocean, rather than the Pacific, play the dominant role in driving variability in the pressure head; namely, the sea level (ocean bottom pressure) changes in the East Siberian Sea sector. They suggest that westward surface winds reduce sea level in this area through Ekman transport of water from the East Siberian Shelf to the Arctic Ocean. Eastward winds have the opposite effect. While this influence is present year-round, it was found to be most dominant in summer, explaining approximately two thirds of the Bering Strait variability. In winter, low SLP in the North Pacific plays an additional role by promoting westward winds in the northern Bering Sea, which increases the sea surface height over the Bering Sea Shelf, in turn driving a northward flow through the strait.

Our aim of shedding further light on the complex interplays between the heat transport, the volume transport, and atmospheric circulation patterns makes use of monthly heat transports, volume transports, and water temperature from a mooring (A3) in the strait, sea surface temperatures (SSTs), SLP, and 10-m winds. Data sources are discussed below. Results are divided into (1) general characteristics of the volume and heat transport, (2) links between the volume transport and variability in SLP and wind patterns, and (3) case studies.

3. Data Sources

We use estimates of monthly averaged ocean volume transport (in Sv), water temperature (°C), and heat transport (TW, relative to −1.9°C) as calculated from the A3 mooring data in the Bering Strait for the periods September 1990 through September 1992 and August 1997 through June 2017 (with the exception of June 1999 for which there are no data). These monthly averages (available at psc.apl.washington.edu/BeringStrait.html) are a product of the Bering Strait Arctic Observing Network project and are calculated from hourly data using methods described in Woodgate (2018).

We use not only the A3 monthly times series of the total volume transport "as is" (i.e., TOTALtrans) but also (for the periods 1991–1992 and 1997–2016) separate time series of the components of the total volume transport associated with (1) the pressure head (referred to below as PHtrans) and (2) local winds in the strait (i.e., WINDtrans), as calculated by Woodgate (2018). These time series are the same as those used by Peralta-Ferriz and Woodgate (2017). WINDtrans is the component of TOTALtrans correlated with the 10-m wind at heading 330° in the strait, the heading found empirically to have the greatest correlation with the flow in the strait. The part that remains after removing WINDtrans is the PHtrans component, an estimate of the pressure head-forced component of the throughflow. Winds for this calculation were taken from the National Centers for Environmental Prediction R1 (NCEP-R1) reanalysis. Measurements from the A3 mooring (which is located at approximately 66.33°N, 168.96°W, ~35 km north of the Bering Strait proper; see Figure 1) have been found to give a reasonable estimate of the non-ACC portion of the total throughflow through the strait (Woodgate et al., 2015). The 1992–1997 gap in the A3 time series reflects prior modifications of the array. The heat flux at A3 is calculated from lower layer (~45-m depth) measurements of temperature and velocity (Woodgate et al., 2010).

The midstrait mooring A3 is considered a "climate site," as it provides a useful average of water properties in the two channels of the strait (Woodgate, 2018). However, the basic calculated heat flux from A3 data is known to underestimate the total Bering Strait heat flux, because it does not capture the contribution from the seasonal (warm) ACC and the effects of vertical stratification of the water column (Woodgate et al., 2010; 2015; Woodgate, 2018). The ACC and stratification are estimated to add ~ 2×10^{20} J/year to the heat transport (ibid.). While seasonal/interannual variability in the effects of stratification can be roughly estimated from SST data (Woodgate et al., 2010), in situ data from the ACC are available only since 2001, and then intermittently. Thus, to be able to consider the throughflow data set back to 1990 consistently, we do not here include the ACC and stratification contributions. While this is perhaps an obvious limitation of our

study, note that prior work has not found significant trends in the ACC or in SST over the periods considered (Woodgate, 2018; Woodgate et al., 2012). Moreover, prior work (Woodgate, 2018) has found significant and high correlations ($r \sim 0.8$ or greater) between annual mean ACC transports and temperatures and the transports and temperatures of the main channel flow, and thus, variability in the total heat flux is likely highly correlated with heat flux as estimated from the main channel flow. The estimated remaining uncertainty (i.e., that due not to the systematic effects but due to the time variability over the period averaged) in the monthly mean temperature, volume transport, and heat transport, calculated from the variance of hourly data over the month using an integral time scale to determine the effective degrees of freedom (Woodgate, 2018), can also be substantial. While estimated uncertainty in monthly mean temperatures is small in winter (generally less than 0.1 °C) when the water is near its salinity-adjusted freezing point, in summer it may exceed 0.5 °C. This reflects the large small time scale variability of temperature. Similarly, uncertainties in the monthly mean volume transport are typically in the range of 0.1 to 0.6 Sv, while those in the heat transport typically range from 0.1 to over 10 TW, again smallest in winter (Woodgate, 2018).

To examine atmospheric circulation patterns, fields of SLP and 10-m wind were extracted from the NASA MERRA2 reanalysis data set (the Modern Era Retrospective-analysis for Research and Applications; Gelaro et al., 2017). MERRA2 output has a spatial resolution of 0.5° latitude by 0.625° longitude. Fields used in this study are available on an hourly basis. We make use of monthly averages. Winds in the strait are computed as monthly averages of the meridional wind averaged between 65–67°N latitude and 168–170°E longitude, cosine weighted by latitude. (As discussed later, other wind angles were also investigated but did not change the conclusions of the paper.) Zonal winds (cosine weighted) in the East Siberian Sea are averaged within the region of maximum correlation with the volume transport identified by Peralta-Ferriz and Woodgate (2017) using the summer time series of the zonal wind velocity and PC1 of the GRACE ocean bottom pressure anomalies (75–80°N, 140–180°E). Both these regions are marked on Figure 1. Comparisons of NCEP-R1 and MERRA2 10-m winds show that they are very similar in the Bering Strait region.

SST anomalies are assessed from the Advanced Very High Resolution (AVHRR)-only version of the NOAA High-resolution Blended Analysis of Daily SST product (Reynolds et al., 2007). We also employ the monthly index of the PDO (Mantua et al., 1997) obtained from the University of Washington and a monthly index of the seasonally variable Arctic Oscillation (AO), calculated as the leading EOF of monthly MERRA2 SLP anomalies north of 40°N on an equal-area grid. Following Ogi and Wallace (2007), the AO is calculated independently for each month of the years 1980–2018.

4. Seasonality and Variability

4.1. General Characteristics

To get a sense of the seasonality and variability in the total volume transport, heat transport (relative to a water temperature of −1.9 °C), and water temperature at the A3 mooring, we find it is useful to express the mooring data in heat maps (Figure 2). As is known (see Woodgate, 2018 for review), there is a clear seasonal cycle to temperature, volume flux, and heat transport. Consequently, the heat transport is generally largest in the summer and smallest in the winter, when the temperature of the water is close to the freezing point (Woodgate et al., 2005b). The volume transport exhibits a less pronounced but nonetheless still seasonal cycle, with more frequent southward flow in winter (Woodgate et al., 2005b). However, there are two months in the record (November and December 2005) when the monthly mean volume transport was negative (southward). As noted, upward trends in annual averages have been documented over the period of record in both the volume and heat transport, the latter largely driven by changing volume transport (Woodgate, 2018; Woodgate et al., 2012). While interannual change is of considerable interest, our focus is on the monthly variability.

Another way of viewing this monthly variability is to use Z scores (anomalies from the record length monthly mean, divided by the standard deviations of the monthly value for each month; Figure 3). This shows the recent warming (Woodgate, 2018)—most of the largest positive anomalies in the heat transport have been in the last few years of the record. Of particular interest (examined later as a case study) is October 2016. This month yielded the highest monthly mean heat transport in the entire A3 record (56 ± 13 TW), coincident with both the highest monthly mean volume transport in the entire

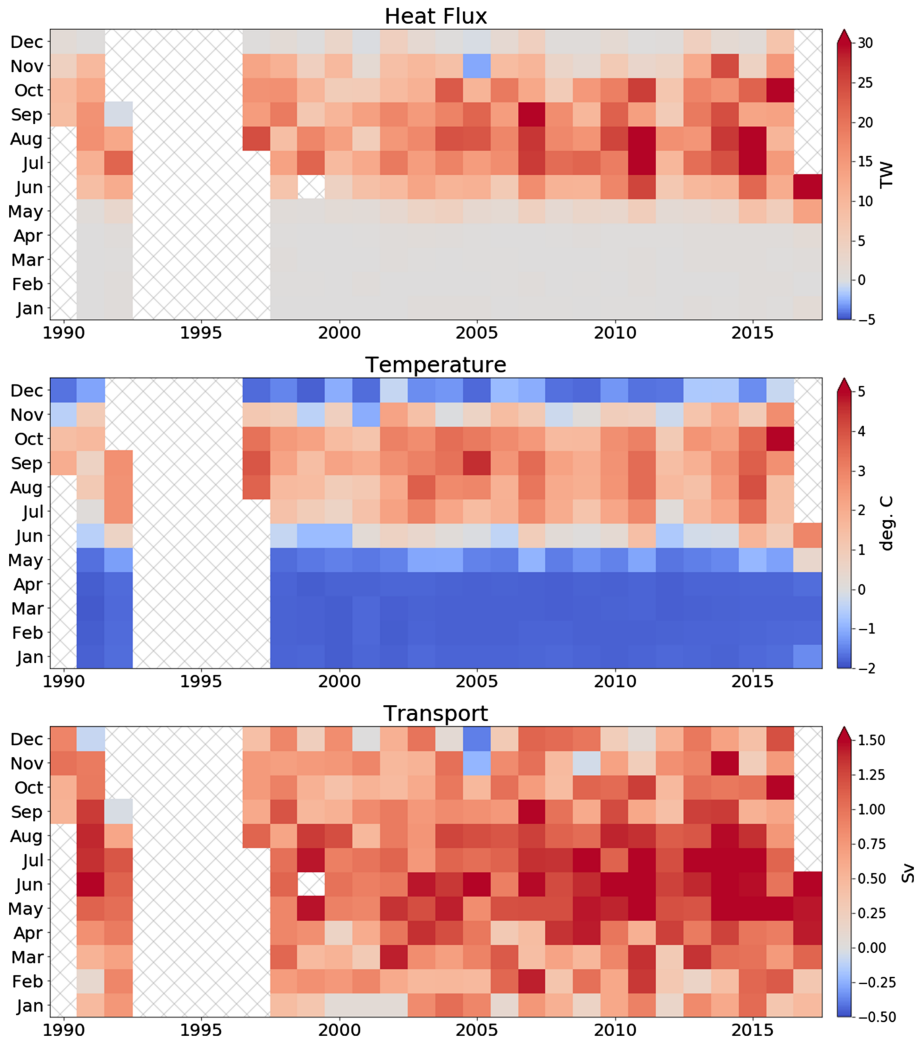

Figure 2. Monthly averaged Bering Strait heat transport (top), water temperature at depth at mooring A3 (middle), and total volume transport (bottom). Crosshatching indicates missing data.

record (2.0 ± 0.5 Sv) and the highest monthly mean water temperature on record at the mooring (5.3 ± 0.2 °C; Woodgate et al., 2017).

4.2. SLP Fields and Local and Remote Winds

As described earlier, the two primary factors generally considered to control the volume transport are local winds directing flow through the Bering Strait and the pressure head difference between the North Pacific Ocean and Arctic Ocean (Stigebrandt, 1984; Aagaard et al., 1985; Roach et al., 1995; Woodgate et al., 2005; Aagaard et al., 2006; Danielson et al., 2014; Woodgate, 2018).

As a start to looking at relationships with atmospheric circulation, Figure 4 shows composites of SLP and 10-m wind anomalies corresponding to the 15 highest and 15 lowest PHtrans values (i.e., transport associated with just the pressure head term) in each 3-month season along with the composite differences. For example, for summer, comprising the months June, July, and August, we looked through all individual monthly values of PHtrans, selected the 15 largest, and compiled SLP and wind anomaly values based on those months. We did the same for the 15 lowest PHtrans values and then computed difference fields. SLP and wind anomalies are computed with respect to SLP averages at each grid cell for each season over the period 1990–2016. Statistical significance of the SLP anomalies was determined for each season using a Monte Carlo simulation. An ensemble was generated of 1,000 composites of 15 months randomly selected from all months in a given season. Upper and lower confidence levels for the observed seasonal SLP composite

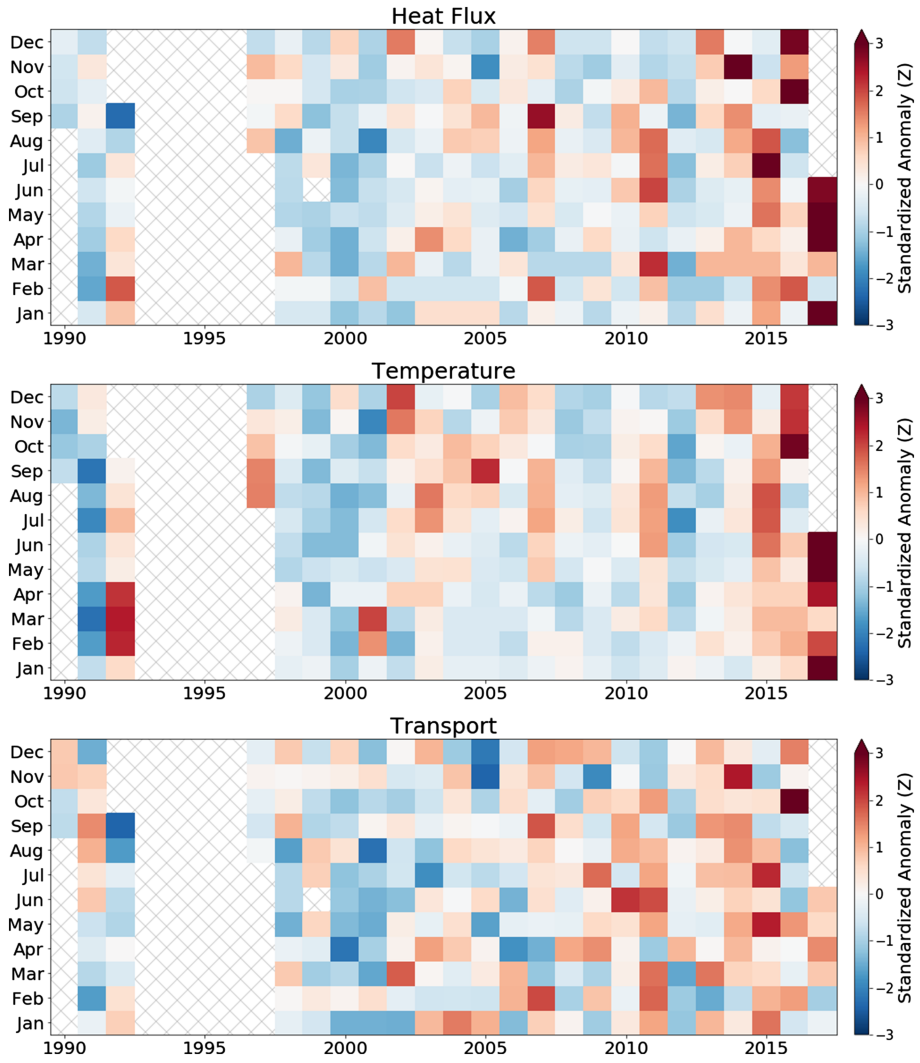

Figure 3. Standardized anomalies (*Z* scores) in the Bering Strait heat transport (top), water temperature at the mooring (middle), and total volume transport (bottom). Crosshatching indicates missing data.

anomalies were estimated based on the 97.5th and 2.5th percentiles of the 1,000 SLP composite anomalies from the simulation. Because we are examining SLP associated with extremes, it is not surprising that anomalies over most of the mapped region are significant at the 95% level.

In support of Peralta-Ferriz and Woodgate (2017), in all seasons, the high PHtrans composite features positive anomalies in SLP over the central Arctic Ocean that favor westward wind anomalies in the East Siberian Sea region (winds will be further examined below). An opposite pattern is found with the low PHtrans composite, featuring negative pressure anomalies over the central Arctic Ocean that favor more eastward wind anomalies over the East Siberian Sea region. This contrast is very clear in the composite difference maps.

Corresponding composites for WINDtrans in the strait follow in Figure 5 (i.e., transport associated with the local winds). The most visually striking plots are those for winter, at which time the local wind effect is known to dominate (Woodgate et al., 2005b). Large WINDtrans in the strait is favored with positive pressure anomalies centered south of the Aleutians (more northward winds on the west side of the high pressure anomaly) paired with somewhat below average pressure over the Arctic Ocean. Low WINDtrans in winter is favored by negative pressure anomalies south of the Aleutians and positive anomalies over the Arctic Ocean. The contrast is again very clear in the composite difference maps. The same type of contrast is evident for spring, but the pressure anomalies are less pronounced. In summer, when the effects of local winds are

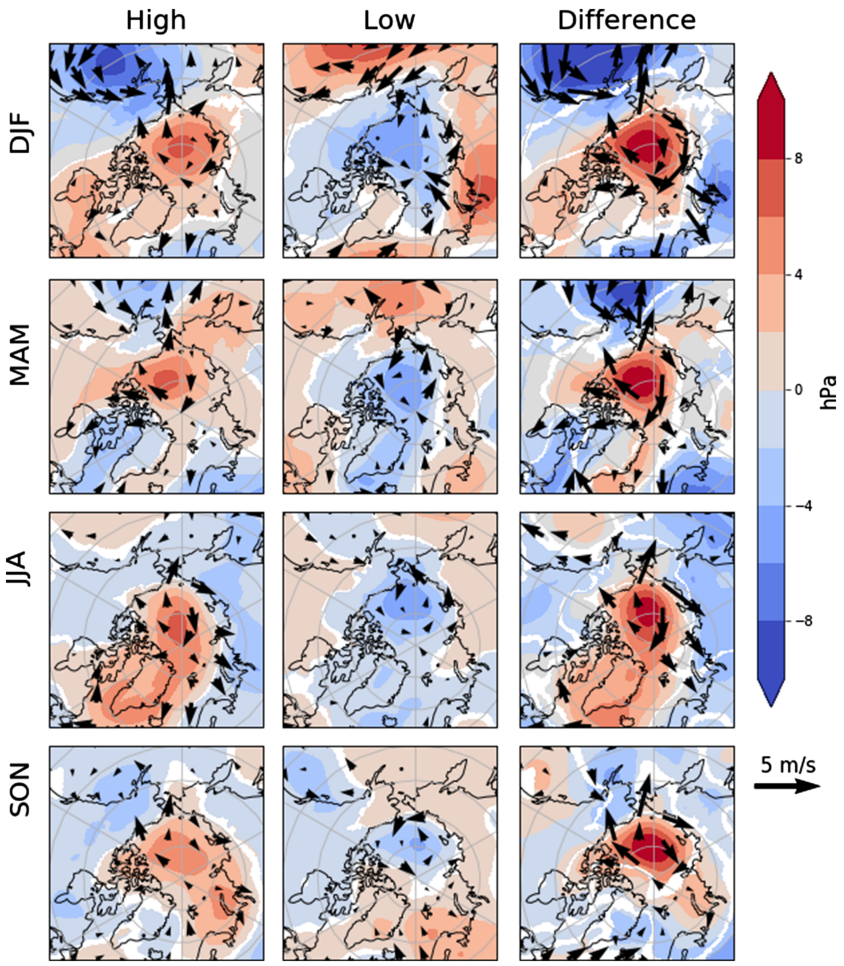

Figure 4. Composite sea level pressure and 10-m wind anomaly fields for the 15 largest (left) and the 15 smallest (right) individual 3-monthly PHtrans for months in winter (December through February, DJF), spring (March through May, MAM), summer (June through August, JJA), and autumn (September through November, SON) and the composite differences (high minus low). Regions with significant pressure anomalies at the 95% level are shown in color. Nonsignificant regions are in white. Anomalies are computed with respect to averages for each season over the period 1990–2016. Wind anomalies are only shown for ocean grid cells.

known to be generally weak, pressure anomalies that could influence winds in the strait are small. The pattern for a large WINDtrans in autumn is strikingly different from the winter pattern. While in winter, up-strait winds are favored by positive pressure anomalies centered south of the Aleutians and above average SLP over the Arctic Ocean, in autumn, up-strait winds stem from the center of the composite mean low pressure anomaly lying just to the west of the Bering Strait. Small WINDtrans in autumn links to a pattern of weak positive anomalies west of the strait.

When seasonal SLP composites are compiled for the 15 highest and 15 lowest individual monthly TOTALtrans values (sum of the pressure head and local wind components; not shown), we only see a clear contrast between positive and negative pressure anomalies over the central Arctic Ocean in the summer. Composites for the other seasons are not clearly interpretable. This is explained by the mixing of circulation patterns that influence the pressure head and local wind components of the transport. In summer, the variability in zonal winds in the East Siberian Sea dominates variability in the total volume transport through its effect on the pressure head. In other seasons, the total transport is variously driven by either remote or local winds (or both in tandem), which are associated with different circulation patterns.

Turning attention to the winds themselves helps to illustrate these points. We start by examining scatterplots of the meridional wind in the Bering Strait and the zonal wind in the East Siberian Sea, averaged over the

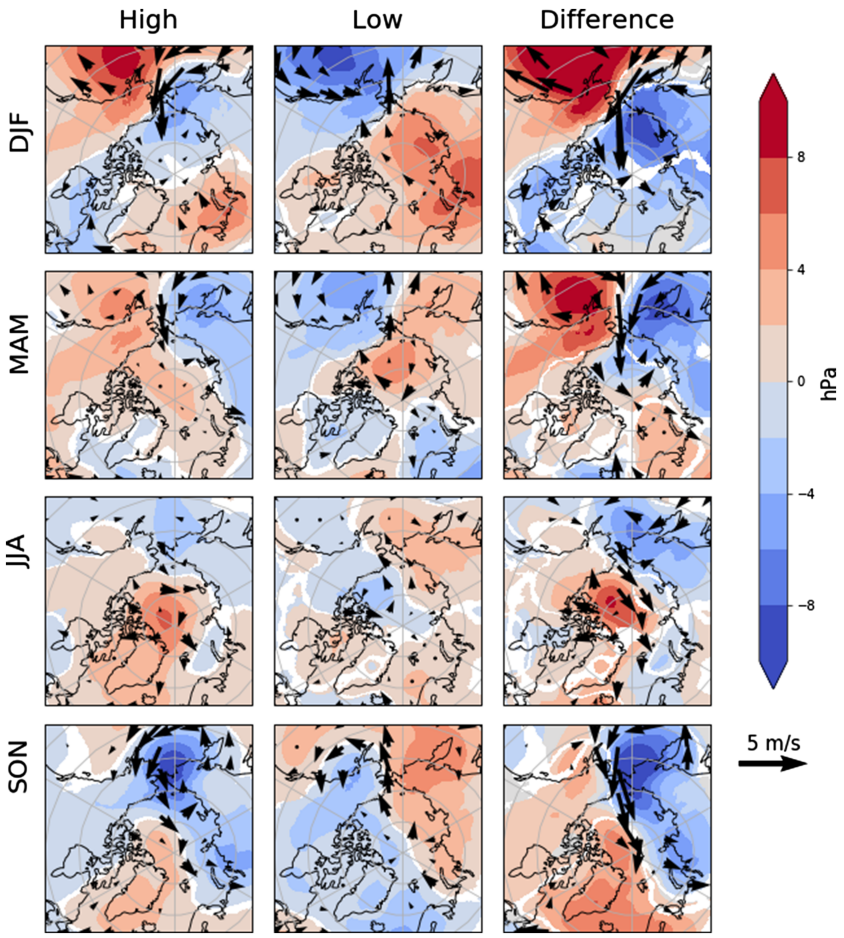

Figure 5. Composite sea level pressure and 10-m wind anomaly fields for the 15 largest and the 15 smallest individual monthly WINDtrans through Bering Strait for months in winter (December through February, DJF), spring (March through May, MAM), summer (June through August, JJA), and autumn (September through November, SON) and the composite differences (high minus low). Regions with significant pressure anomalies at the 95% level are shown in color. Nonsignificant regions are in white. Anomalies are computed with respect to averages for each season over the period 1990–2016. Wind anomalies are only shown for ocean grid cells.

regions defined in Figure 1, against TOTALtrans (pressure head plus the local wind), along with linear correlations and p values (Figure 6). Recall that these regions correspond to the areas of maximum correlation with the volume transport identified by Peralta-Ferriz and Woodgate (2017) using the time series of the zonal wind velocity and PC1 of the GRACE ocean bottom pressure anomalies.

During summer, TOTALtrans and the zonal wind in the East Siberian Sea correlate robustly (-0.78, $p < 0.05$) while the relationship with the meridional wind in the Bering Strait is very weak. By contrast (as found by several prior authors; see Woodgate, 2018, for review), TOTALtrans is more strongly correlated with the meridional winds in Bering Strait (0.70, $p < 0.05$) during the winter. The correlation with the zonal wind in the East Siberian Sea, while not high, is still significant. The same holds true for spring. In autumn the correlations with the local and remote winds are about equal (0.62 and -0.69, respectively, both with $p < 0.05$). Table 1 provides mean values of the local and remote winds for the 15 highest and 15 lowest 3-monthly TOTALtrans values by season; significance testing follows the same basic Monte Carlo procedure used to assess the SLP composites discussed earlier. Note how in summer the contrasts in zonal winds in the East Siberian Sea are statistically significant while those for the local wind in the strait are not. All other composite anomalies in Table 1 are significant except for East Siberian Sea zonal winds during low spring volume transport.

Past analyses (Woodgate, 2018 and references therein) find that the highest correlation between Bering Strait volume transport and local wind field is for the wind with a heading of 330° true. This is locally

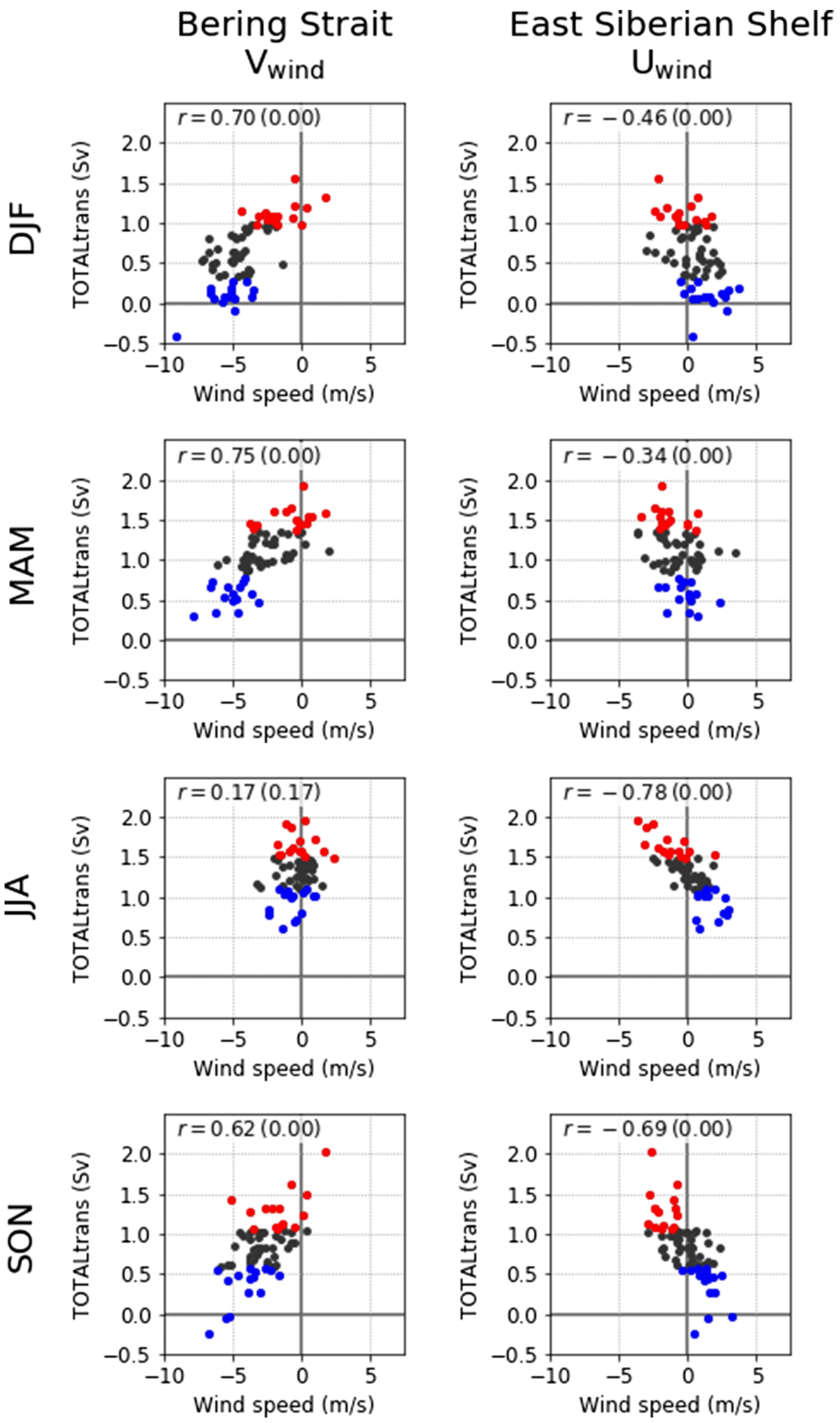

Figure 6. Relationship between TOTALtrans, meridional winds in the Bering Strait, and zonal winds in the East Siberian Shelf. Correlation coefficients are shown in the top left of each panel along with *p* values in parentheses. Red circles are the 15 highest monthly transports. Blue circles are the 15 lowest monthly transports.

Table 1
Mean Winds for the 15 Highest and 15 Lowest Monthly Total Volume Transports (TOTALtrans)

Season	Bering Strait meridional wind, high volume transport (m/s)	East Siberian Sea zonal wind, high volume transport (m/s)	Bering Strait meridional wind, low volume transport (m/s)	East Siberian Sea zonal wind, low volume transport (m/s)
Winter	**−1.5**	**−0.4**	**−5.5**	**1.4**
Spring	**−0.8**	**−1.4**	**−5.2**	0.2
Summer	−0.2	**−1.4**	0.7	**1.6**
Autumn	**−1.6**	**−1.8**	**−4.1**	**1.3**

Note. Significant values are shaded in bold, non-significant values are shaded in gray.

close to the alignment of the channel of the strait, which is to the north-northwest at mooring site A3. The maximum correlation with the heat transport is quite similar. We assessed the sensitivity of correlations between the TOTALtrans and rotated winds. While the highest correlation with winds in the Bering Strait (based on the MERRA2 data, which have a higher spatial resolution than the data used by Woodgate, 2018) is with winds at 349° true, correlations obtained are very close to (~0.05) those calculated using just the meridional wind. However, we do not believe this difference to be significant but more likely reflects the different resolution and level of wind products used.

The same approach was used to assess correlations with winds in the East Siberian Sea sector. There, correlations with the transport are slightly (~0.05), but not significantly higher, with winds at 287° true as opposed to purely zonal. As discussed in Woodgate (2018), the northward flow through the strait is best correlated with the along-strait (approximately northward) wind, not the across strait (approximately eastward) wind, as one might expect from an Ekman transport model of the throughflow. It is reasoned (Woodgate, 2018) that this is due to the along-strait wind setting up (by local Ekman transport in the strait) an across strait sea surface height gradient, which then drives the along-strait (approximately northward) flow. Thus, since we are more interested in mechanism than exact correlation values, for simplicity from hereon, we continue to consider relationships to the meridional wind (in the Bering Strait) and the zonal wind (in the East Siberian Sea).

To expand upon results from the scatterplots, monthly point correlations between TOTALtrans and the 10-m meridional and zonal wind components follow in Figures 7 and 8. Coloring is limited to grid cells for which the correlations have an associated p value of <0.05. Consistent with the composite analysis and correlations with the regionally averaged winds, except for the summer months, the strongest correlations between TOTALtrans and meridional winds are in the vicinity of the Bering Strait. This agrees with the known correlation between the local wind and the flow (e.g., Woodgate, 2018). Building on previous results, a noteworthy point about the meridional winds in the strait is that, as assessed over the period 1990–2017, northward winds occurred on only 17% of all months (1990–2017). Also of interest is that average up-strait winds as assessed over all months (0.9 m/s) are considerably weaker than average down-strait winds (3.6 m/s). Both these points support previous statistical analysis of the Bering Strait wind field; Woodgate (2018) shows that monthly mean winds are very rarely northward (their Figure 11), and only in summer months is the climatological mean northward. For the zonal wind, the strongest correlations (which are negative, denoting that a westward wind coincides with northward volume transport, as one would expect in a standard Ekman response) are found in June through September not just in the East Siberian Sea region but all along the Siberian coastline (Figure 8). The pattern is also fairly strong in December and January. In January, a region of high correlations is also found in the North Pacific.

A few words on persistence are warranted. In all months but July, the lag −1 correlation of TOTALtrans (the correlation between the volume transport for a given month and the previous month) is low and not statistically significant, and in July the lag −1 correlation is only 0.51 ($p = 0.02$). This is consistent with higher time resolution results of Woodgate et al. (2005), which suggest that the wind-water correlation is highest at lags <6 hr. The lack of month-to-month memory in the correlation points to a lack of persistence in atmospheric circulation patterns (see next section). It also argues that adjustments in the pressure head difference occur on time scales less than a month, consistent with the Peralta-Ferriz and Woodgate (2017) results, which find the strongest correlations between ocean bottom pressure and flow in the same month. The summer atmospheric pattern (not shown) features positive SLP anomalies over the central Arctic Ocean

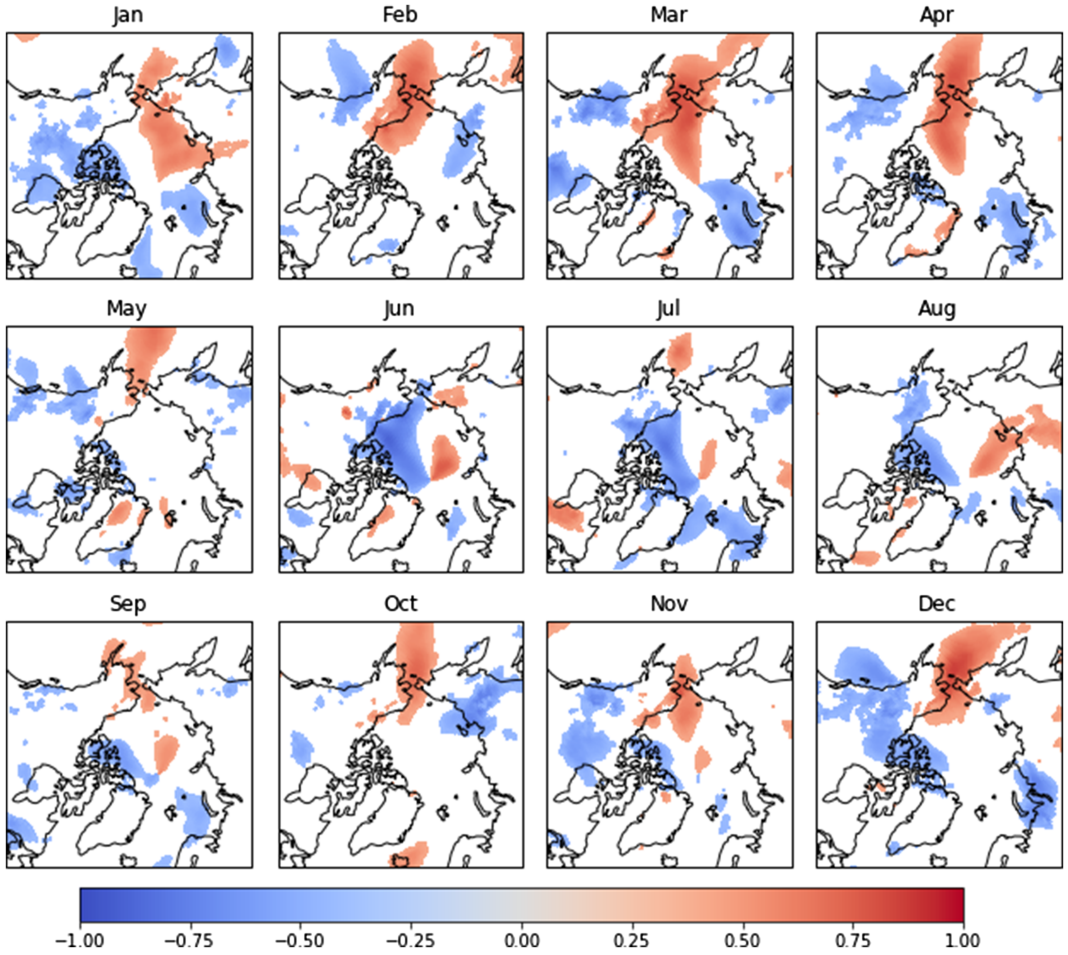

Figure 7. Monthly point correlations between the monthly Bering Strait TOTALtrans and the 10-m meridional wind. Correlations with p values of >0.05 are not shown.

associated with greater TOTALtrans in the subsequent month. However, the correlation patterns with winds are much weaker compared to the same-month correlations shown in Figures 7 and 8.

How are the high and low PHtrans and WINDtrans months distributed among the overall distribution of TOTALtrans values? For example, are there high PHtrans months that are associated with low TOTALtrans? To address this issue, we compiled a parallel coordinate plot (Figure S1 in the supporting information) to show how rankings of PHtrans and WINDtrans relate to TOTALtrans. Values for these transports are plotted on the three (parallel) y axes. Points for the same months are joined by lines to retain the relationships between these values. The 15 highest and lowest TOTALtrans months are depicted in color, while the remainder are depicted in gray. In summary, there are no high PHtrans associated with low TOTALtrans, but there are some months with PHtrans exceeding TOTALtrans. However, high PHtrans in these months are countered by negative (to the south) WINDtrans, reducing TOTALtrans.

4.3. A Larger Context

The Bering Strait heat transport is (by definition here) tied to the volume transport, and (as already introduced) links have been established between the heat transport and sea ice conditions in the Chukchi Sea (Ahlnas & Garrison, 1985; Fedorova & Yankina, 1963; Paquette & Bourke, 1974; Serreze, Crawford, et al., 2016; Spall, 2007; Woodgate et al., 2010; Woodgate et al., 2015). In turn, the strength of the summer volume transport links to zonal winds in the East Siberian Sea. It is very interesting that the variability in zonal winds in this area is the regional expression of the contrast between anomalously cyclonic and anticyclonic

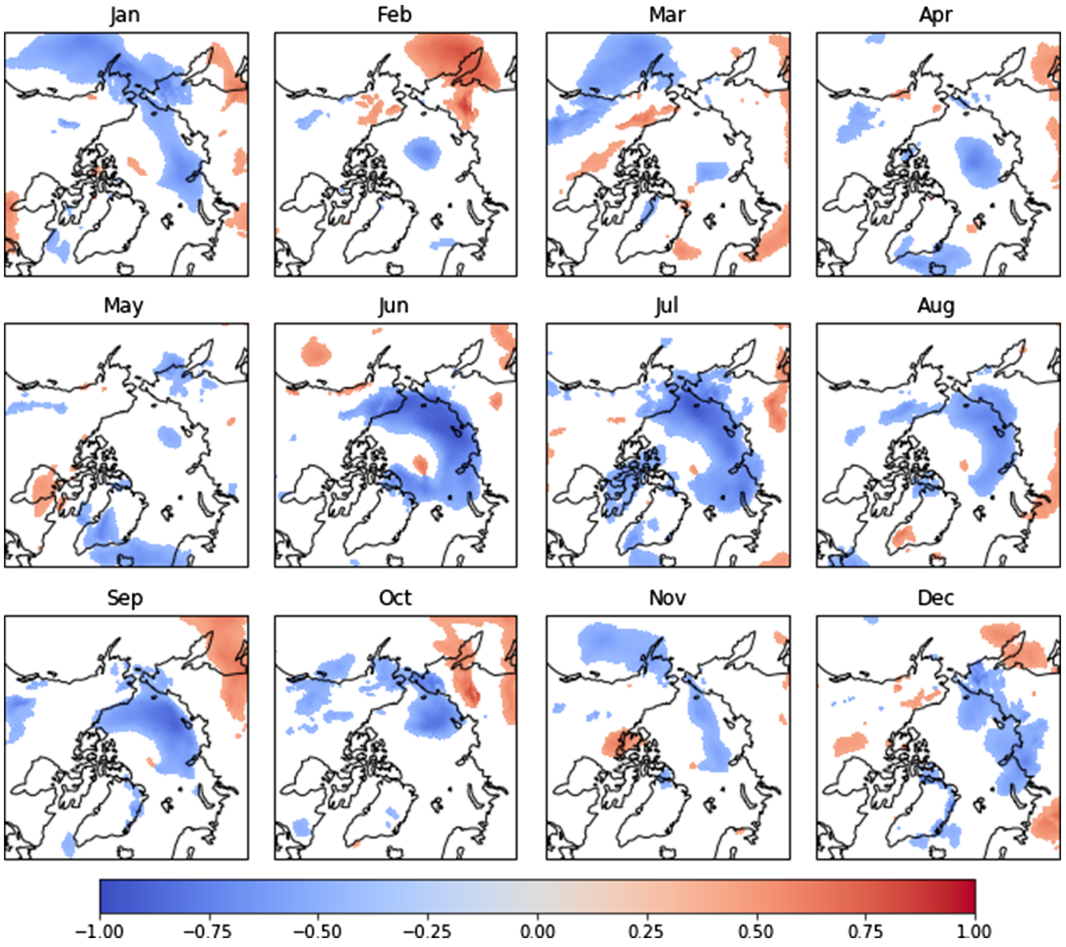

Figure 8. Point correlations between the monthly Bering Strait TOTALtrans and the 10-m zonal wind. Correlations with p values of >0.05 are not shown.

conditions over the central Arctic Ocean (Figure 4), which is known to influence September ice extent for the Arctic as a whole (e.g., Ogi & Wallace, 2007; Overland et al., 2012; Serreze et al., 2016).

The contrast between cyclonic and anticyclonic conditions at the surface relates to variability in the strength of the circumpolar vortex at higher atmospheric levels. Anticyclonic conditions at the surface are favored when the vortex has a meridional structure, with an upper-air ridge (seen clearly at the 500 hPa level, for example) extending into the northern Beaufort Sea. When the vortex is more zonally symmetric, the surface high is absent. Instead, there is frequent migration of vertically stacked (barotropic), cold-cored cyclones into the central Arctic Ocean, which often results in a mean low in monthly averaged (or sometimes summer-averaged) SLP fields (Screen et al., 2011; Serreze & Barrett, 2008, 2011). When anticyclonic conditions are dominant over the central Arctic Ocean (corresponding to westward winds in the East Siberian Sea), tropospheric air temperatures tend to be above average, promoting more melt. Dynamically, a more anticyclonic sea ice circulation also favors reduced extent because the ice motion tends to be slightly convergent. When low pressure dominates (corresponding to eastward winds in the East Siberian Sea), tropospheric temperatures tend to be below average, meaning less melt, and cyclonic ice motion favors divergent ice motion, spreading the ice out to cover a larger area. Precipitation associated with the cyclones that migrate into the central Arctic Ocean may fall as snow, increasing surface albedo, also inhibiting melt (Screen et al., 2011).

Ogi and Wallace (2007) capture some of these pressure relationships in the framework of the "summer Arctic Oscillation" (AO) mode of variability. Compared to its winter counterpart, which has a "center of action" focused near the Icelandic Low, the center of action of the summer AO is focused over the

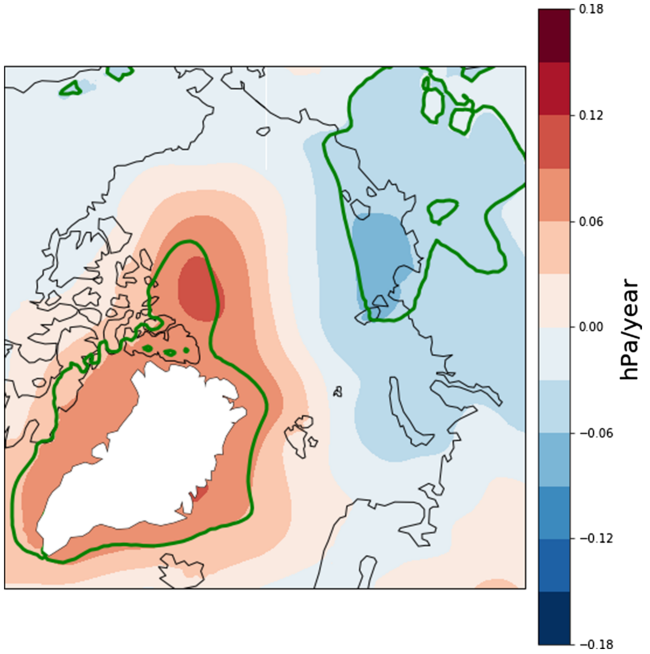

Figure 9. Linear trends in summer (June through August) sea level pressure over the period 1980–2017. Trends in areas enclosed by the green lines are statistically significant ($p < 0.05$). Values over the Greenland ice sheet are masked.

central Arctic Ocean. Cyclonic conditions over the central Arctic Ocean are associated with the positive phase of the summer AO, and anticyclonic conditions with the negative phase. The situation with high pressure over the central Arctic Ocean also corresponds broadly to the high pressure "half" of the "Arctic Dipole Anomaly" (AD) pattern advanced by Wang et al. (2009). In this framework, when the AD is present, high pressure over the central Arctic Ocean pairs up with low pressure over northern Eurasia. The pattern seems to have been best developed in the summer and early autumn of 2007, corresponding to the second lowest September sea ice extent in the satellite record.

Overland et al. (2012) argued that the high pressure, anticyclonic summer pattern favoring low September sea ice extent became increasingly prominent over the period 2007–2012. Serreze, Stroeve, et al. (2016) revisited this through an analysis of summer-averaged (June through August) SLP fields for the period 1979–2015. An updated trend analysis through 2017 (Figure 9) points to statistically significant increases in pressure north of the Canadian Arctic Archipelago, attended by significant negative trends over northern Eurasia, meaning stronger and/or more persistent westward winds along the Russian Arctic coast. However, this is most prominent not over the East Siberian Sea but further westward over the Laptev Sea. The small areas over Alaska passing the significance test are likely noise. A closer analysis by Serreze, Stroeve, et al. (2016) reveals that the trend pattern is dominated by the most recent decade they examined (2006 through 2015). Suggestively, the heat maps in Figure 2 hints that summer volume and heat transports have been larger in the later part of the record, which may relate to observed trends in the large-scale SLP pattern. However, in the most recent summers, the trend in SLP has broken down; strongly cyclonic summer patterns have instead prevailed in the summers of 2016 and 2017 and to a lesser extent in 2018. Despite the relationship indicated by these results between the AO and Bering Strait throughflow, there is limited persistence in large-scale atmospheric patterns (Table 2). A weak but significant correlation exists between the AO index in consecutive months, but no significant correlation exists for a 2-month lag, for consecutive seasons, or for consecutive years.

As noted earlier, Woodgate (2018) finds warming trends in Bering Strait waters at the A3 mooring in some summer months. In turn, some of the largest Bering Strait heat transports have occurred in the most recent part of the A3 record, and these are clearly (and unsurprisingly) associated with high water temperatures. As suggested from Figure 10, which compares the mean spatial pattern of monthly SST anomalies (the average of all monthly anomalies) for the periods 2008–2013 and 2014–2017, these findings tie into a larger-scale pattern of recent ocean warming. The two periods in turn correspond (perhaps unsurprisingly) to a shift in the Pacific Decadal Oscillation (PDO; the dominant pattern of monthly SST variability in the North Pacific; Newman et al., 2016), from a primarily negative mode to a primarily positive mode. Clement et al. (2005) found weak statistical links between the PDO index and Bering Strait transport ($r \sim 0.5$ for 13-month averages between 1979 and 2001) in a coupled sea ice-ocean model simulation. Our own analysis finds spotty correlations between the monthly PDO index and the same month water temperature in the strait based in the A3 mooring record, ranging from 0.29 (January, $p > 0.05$) to 0.76 (November, $p < 0.05$). It is not surprising that the correlations are spotty. First, the PDO is defined on the basis of SST, while the water temperature in the strait is measured at depth. Second, Bering Strait is a small region on the northern fringe of the very large ocean region (the Pacific poleward of 20°N) that the PDO index is based upon. Even SSTs in the Bering Strait region are hence unlikely to consistently correlate with the PDO index. Third, in January, the Bering Strait temperatures are around freezing, due to ice formation, which is not present

Table 2
Persistence of Seasonally Variable Arctic Oscillation, as Calculated by Lagged Pearson's Correlations (p Values in Parentheses) at 1 to 4 Years, Seasons, or Months for the Period 1980 to 2018

	Lag time for correlation			
AO calculation	1 period	2 periods	3 periods	4 periods
Annual average	0.27 (0.10)	0.00 (0.98)	−0.06 (0.74)	−0.09 (0.61)
Seasonal average	−0.04 (0.61)	0.14 (0.09)	0.10 (0.20)	0.06 (0.44)
Monthly average	0.25 (<0.01)	0.06 (0.18)	0.05 (0.29)	−0.02 (0.63)

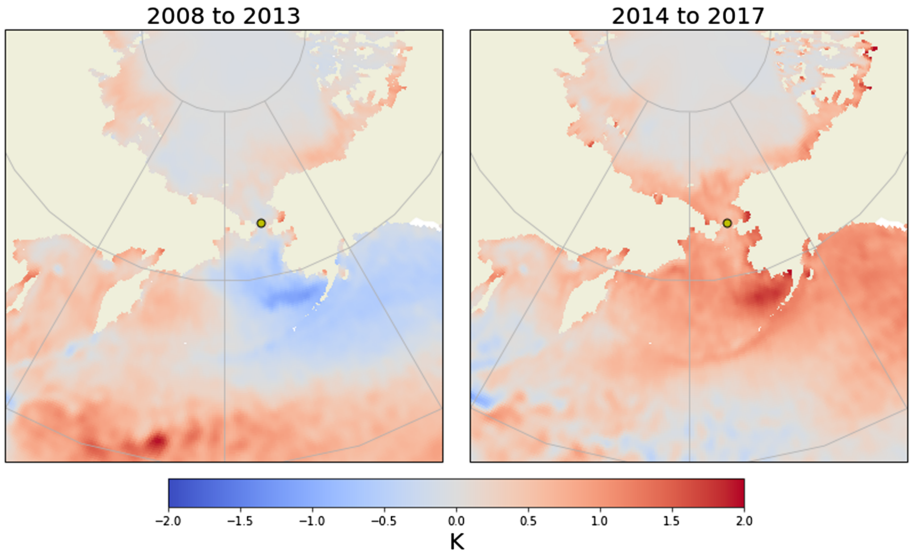

Figure 10. Monthly sea surface temperature anomalies averaged for the periods 2008–2013 and 2014–2017 with respect to 1981 to 2018 monthly climatologies.

in most of the Pacific. Furthermore, attempts to relate the PDO index to the heat transport are of course further muddied in that the Bering Strait heat transport is also a function of the volume transport. The cause of the SST variability that defines the PDO index remains largely unknown.

5. Case Studies

To help illustrate the varying contributions to the volume transport by the local and remote winds, how these relate to SLP patterns, and how the volume transport relates to the heat transport, it is instructive to examine some case studies, focusing on fields of 10-m wind vectors, SLP anomalies, and SST anomalies. Anomalies are with respect to the period 1990–2016 corresponding to the month of each case study. For each case study, we also computed the monthly average zonal wind in the East Siberian Sea and the meridional wind in the Bering Strait region. We then assessed if the wind values for the month and year being examined fell outside of the 97.5th and 2.5th percentile values of all regional average wind values for the month and adjacent months over the period 1990–2016. If falling outside of these bounds, the value is taken as statistically different from the mean. Table 3 summarizes characteristics of the five case studies.

Table 3
Characteristics of the Five Chosen Case Studies

	Case 1	Case 2	Case 3	Case 4	Case 5
Date	September 2007	October 2016	November 2016	December 2016	November 2005
Why chosen	Highest September volume and heat transport on record	Highest volume and heat transport (of all months) on record	Second highest heat transport (of all months) on record	Highest December heat transport on record	Small southward heat transport
Volume transport and (in parentheses) climatology (Sv)	1.5 (0.8)	2.0 (0.8)	0.7 (0.7)	1.2 (0.5)	−0.2 (0.7)
Heat transport and (in parentheses) climatology (TW)	32.8 (15.2)	56.4 (15.8)	15.1 (7.8)	7.5 (1.8)	−2.7 (7.8)
Temperature and (in parentheses) climatology (°C)	3.5 (2.6)	5.4 (2.5)	2.8 (0.8)	−0.3 (−1.3)	0.6(0.8)
Bering Strait meridional wind and (in parentheses) climatology (m/s)	0.3 (−2.8)	1.7 (−2.6)	−3.3 (−2.9)	−0.5 (−4.1)	−6.7 (−2.9)
East Siberian Sea zonal wind and (in parentheses) climatology (m/s)	−2.8 (0.2)	−2.7 (−0.5)	0.2 (0.0)	0.2 (0.3)	0.4 (0.0)

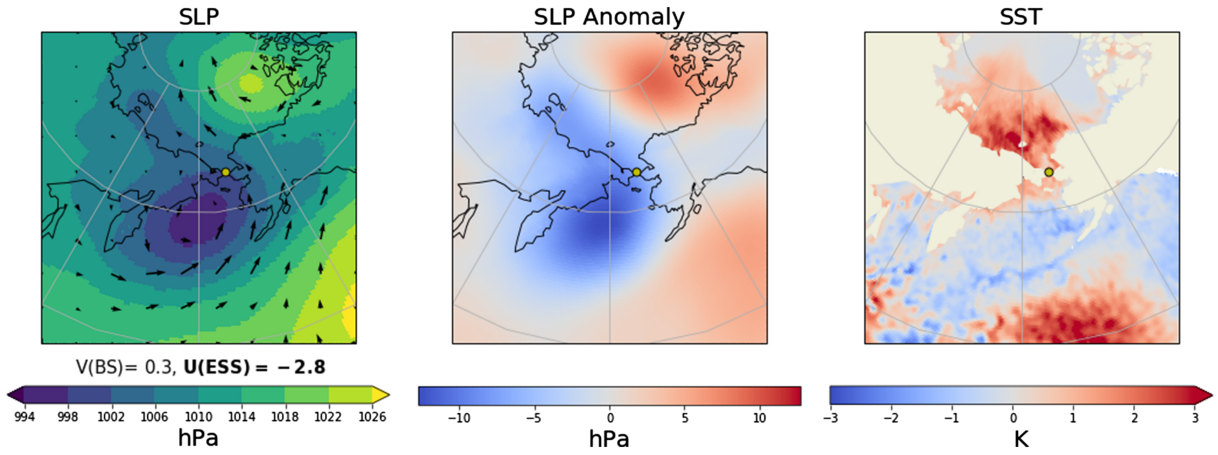

Figure 11. Case Study 1: September 2007. This month had the highest September volume and heat transport in the A3 mooring record (Table 3). Shown are sea level pressure, sea level pressure anomalies, and SST anomalies, along with the meridional wind in the Bering Strait (V (BS)) and the zonal wind in the East Siberian Sea (U (ESS)), in m/s. Statistically significant regional winds are shown in bold text below first panel. Anomalies are with respect to the period 1990–2016 corresponding to the month of the case study.

5.1. Case Study 1: September 2007

We start with the situation for September 2007 (Figure 11). The total volume transport for this month was the largest observed for September (1.5 ± 0.2 Sv), close to twice the climatological average for this month, as was the heat transport (33 ± 5 TW). The water temperature at the mooring was high (3.5 ± 0.2 °C) and about a degree above the climatological average (Table 3), but lower than September 2005 (4.6 ± 0.9 °C). The large volume transport is consistent with the SLP and wind anomaly fields. There was a statistically significant westward wind averaged over the East Siberian Sea (−2.8 m/s). While the regionally averaged wind in the Bering Strait was weak (0.3 m/s) and not different than the mean, it is perhaps notable that it was not opposing the northward flow. The westward wind in the East Siberian Sea region was associated with the combination of an anticyclone centered over the northern Beaufort Sea and Canada Basin and low pressure over the Bering Sea. The SLP and wind pattern suggest that the large heat transport for this month was the result of the combined effects of fairly high water temperatures in the strait and unusually strong (based on the Monte Carlo tests) westward wind in the East Siberian Sea (i.e., the pressure head forcing) and weak winds in the strait. Woodgate (2018) find the annual mean transport in 2007 to have a high PHtrans component (Figure 9 in Woodgate, 2018).

Note also that Bering Strait temperature, volume transport, and thus heat transport were persistently high throughout the summer of 2007 (Figure 3). This occurred in conjunction with a persistent pattern of high SLP over the central Arctic Ocean that yielded westward winds along the East Siberian Sea sector. In the

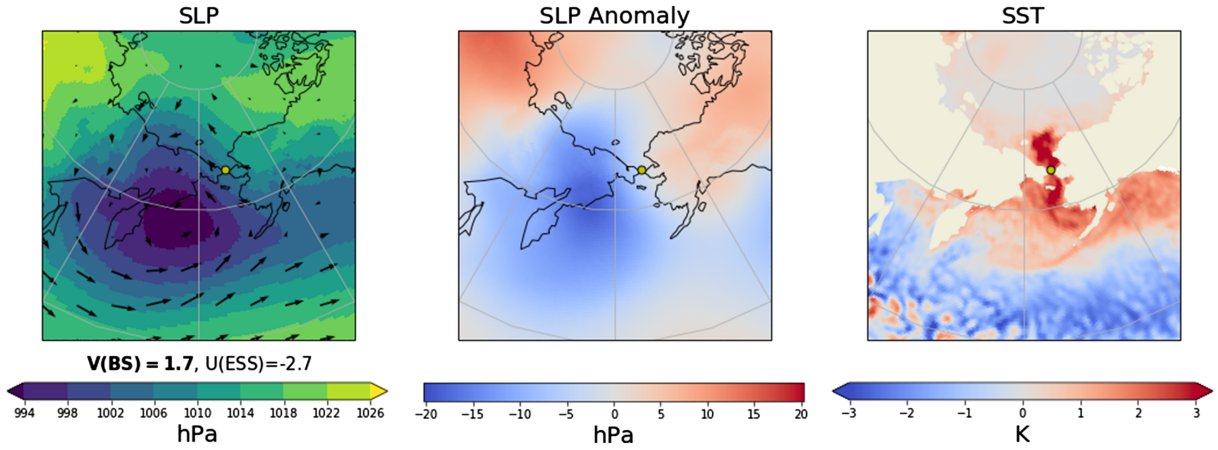

Figure 12. Case 2: October 2016. This month had the highest volume and heat transport in the entire A3 record (Table 3). Variables are the same as in Figure 11.

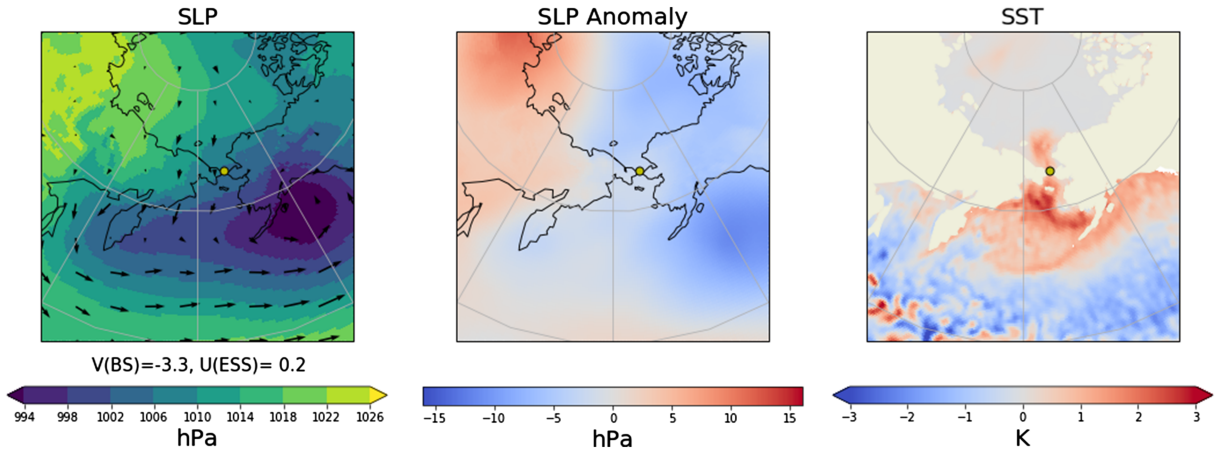

Figure 13. Case 3: November 2016. This month had the second highest heat transport in the A3 mooring record (Table 3). Variables are the same as in Figure 11.

framework of Wang et al. (2009), the pressure pattern in the summer of 2007 represents the prime example the AD pattern, although recall from our previous discussion that such persistence is uncommon.

5.2. Case Study 2: October 2016

Consider next October, November, and December 2016, a 3-month period when heat transports were also unusually high. October 2016 had the highest heat transport in the entire A3 record (56 ± 13 TW), more than 3 times larger than the climatological average, the highest volume transport in the entire record (2.0 ± 0.5 Sv), more than twice climatology, along with the highest water temperature on record for any month (5.4 ± 0.3 °C), 2.4 °C above climatology (Table 3).

The key SLP feature for October 2016 (Figure 12) was the strong low east of Kamchatka—very similar to the situation in Figure 11, but with the low shifted slightly west. In contrast to the situation for September 2007, there was no obvious positive pressure anomaly north of the Beaufort Sea. The position of the low pressure center east of Kamchatka gave rise to uncommonly high meridional wind northward through the strait (1.7 m/s). This was paired with a westward wind in the East Siberian Sea (−2.7 m/s) that, while almost as strong as that for September of 2007, is not statistically different from the mean. This points to a highly variable wind field in this region during October. The record-high heat transport hence appears to have been due to the combination of high water temperatures and northward winds in the Bering Strait and strong winds in the East Siberian Sea.

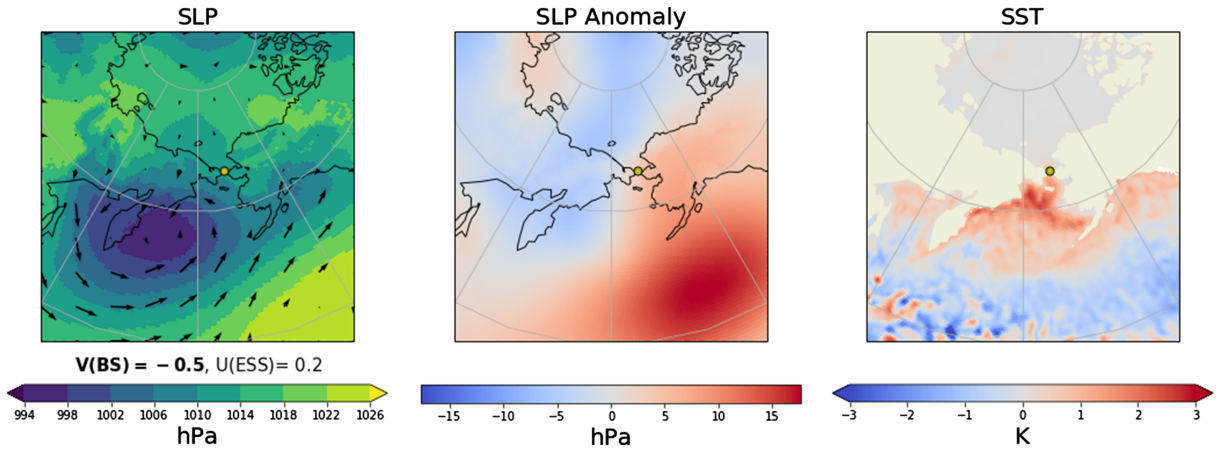

Figure 14. Case 4: December 2016. This month had the highest December heat transport in the A3 record (Table 3). Variables are the same as in Figure 11.

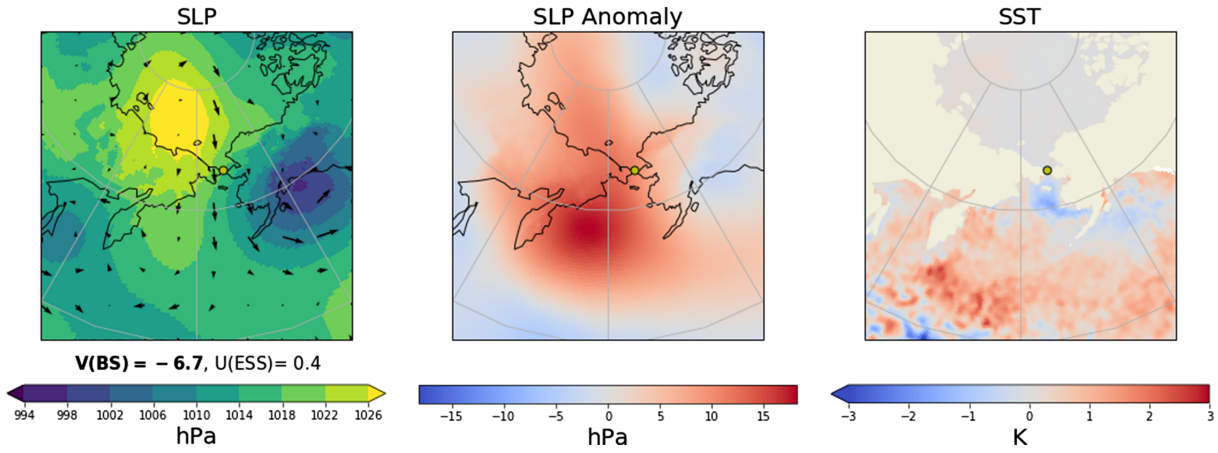

Figure 15. Case 5: November 2005. This month had a small southward (negative) heat transport (Table 3). Variables are the same as in Figure 11.

5.3. Case Study 3: November 2016

Corresponding maps for November 2016 follow in Figure 13. The Bering Strait heat transport for November of 2016 was 15 ± 12 TW, the second highest in the A3 record, about twice climatology (but with a large uncertainty, the highest heat transport was 25 TW during November 2015). The water temperature at the mooring of 2.8 ± 0.5 °C was the highest on record for this month and 2 °C above the climatological average (Table 3). Interestingly, with the month's mean SLP field featuring a low over the Gulf of Alaska, a fairly strong meridional wind was directed down the strait—from north to south (−3.3 m/s). While not statistically different from the mean (again pointing to high variability in the wind field), it opposed the inflow associated with the Pacific to Arctic pressure head difference. The zonal winds in the East Siberian Sea were low. Not surprisingly, the November volume transport of 0.74 ± 0.6 Sv was near average. Hence, the large heat transport for this month appears to simply relate to the warm waters in the strait.

5.4. Case Study 4: December 2016

In December of 2016 (Figure 14), the Bering Strait heat transport was 7.5 ± 3 TW, the highest recorded for a December, more than 3 times larger than climatology. The water temperature at the mooring was −0.3 ± 0.2 °C, the highest on record for this month and a degree warmer than average (Table 3). Neither meridional winds within the strait (−0.5 m/s) and zonal winds in the East Siberian Sea (+0.2 m/s) were significantly different from the mean, suggesting that the large heat transport for this month most likely again relates to the high water temperatures in the strait. However, despite the average winds, the volume transport of 1.2 ± 0.5 Sv was also the highest on record for this month and more than twice climatology. This may be a case for which winds along the Bering Sea shelf region or weak winds within the strait played a contributing role, similar to the results of Danielson et al. (2014) and the winter results of Peralta-Ferriz and Woodgate (2017).

5.5. Case Study 5: November 2005

Finally, it is useful to look at the case of November 2005 (Figure 15), when the volume transport was southward (−0.2 ± 0.5 Sv), yielding a small southward heat transport (−2.7 ± 6 TW); the climatological average is 7.8 TW (Table 3). Note how the anticyclone centered over the East Siberian Sea, combined with low pressure over the Gulf of Alaska, gave rise to a strong and statistically significant wind component southward through the strait (−6.7 m/s). SST anomalies in the vicinity of the strait were slightly negative. This basic pressure pattern persisted through December of 2005, making these the only two months in the A3 record with a southward volume and heat transport. The main cause of this southward heat flux appears to be the anomalously strong southward winds in the strait.

6. Discussion and Conclusions

The oceanic heat transport through the Bering Strait is a highly variable and complex phenomenon, involving variability in both the volume transport and the water temperature in the strait. The volume transport is

most likely tied to constantly changing atmospheric circulation patterns that influence both the Pacific to Arctic oceanic pressure head and meridional winds in the strait. While we have focused here on the role of zonal winds in the East Siberian Sea in driving variability in the pressure head difference, we readily acknowledge that other drivers, notably winds in the Bering Shelf region as identified by both Danielson et al. (2014) and Peralta-Ferriz and Woodgate (2017), can be important, especially in winter and spring, variously reinforcing, partly canceling, or acting independently of the effects of the East Siberian Sea winds. For example, winds along the Bering Shelf may have been a strong driver of the large heat transports observed for December 2016 (our Case Study 4). Note that we have not addressed here annual-scale change, which may offer some additional insights.

An interesting observation with respect to variability in zonal winds in the East Siberian Sea during summer is that they are a regional expression of the known tendency for the atmospheric circulation over the central Arctic Ocean to vary between anticyclonic and cyclonic conditions. This links the Bering Strait volume and heat transports to processes influencing September sea ice extent for the Arctic Ocean as a whole. There is little month-to-month persistence in the total volume transport, which follows from the lack of persistence in atmospheric winds. Nevertheless, the period 1980–2017 saw a summertime trend toward higher pressure over the central Arctic Ocean, favoring increased transports, although low pressure has dominated the central Arctic Ocean over the past several summers.

Some of the most recent large heat transports are associated with high water temperatures in the strait. Of particular note is that autumn of 2016 marks the onset of a multimonth period of anomalous warmth. While warm water persisted through June 2017, the end of the available A3 record, analysis of SSTs point to continued warmth through the end of that year also. This helps to explain the very early sea ice retreat in the Chukchi Sea in the spring and summer of 2017 as well as a very long duration of open water in the Chukchi Sea in autumn 2017. The pattern of late freezeup and early development of open water in this region has subsequently persisted, with the early ice retreat in the spring/summer of 2019 generating considerable interest. It will prove instructive to examine the associated Bering Strait heat transports once the mooring data become available.

If the oceanic heat transport through the Bering Strait could be predicted several months in advance, it could provide an avenue to predicting sea ice conditions in the Chukchi Sea at useful lead times (e.g., the timing of seasonal spring/summer sea ice retreat and autumn ice advance). An obvious challenge is that wind patterns that control the volume transport are highly variable and have limited predictability beyond the 7- to 10-day scale of numerical weather prediction. However, even general information that seasonal climate outlooks might eventually provide, such as the persistence of high or low SLP over the central Arctic Ocean, would be highly valuable. Whether climate warming will be associated with changes in atmospheric circulation patterns that influence the volume and heat transports is an open question. Ocean temperature and SST anomalies, such as those associated with the PDO, tend to have a longer persistence than atmospheric anomalies. However, the Bering Strait region is on the far northern end of the PDO influence, and our initial evaluations suggest that it has limited value. It is reasonable to expect, however, that general ocean warming in coming decades will translate into a larger Bering Strait oceanic heat transport. Indeed, analysis of the A3 mooring data indicates that upward trends are already present in the mooring temperatures in summer (Woodgate, 2018). A greater heat transport, hastening spring/summer ice retreat, would then foster increased seasonal ocean heat uptake (Serreze, Crawford, et al., 2016), further lengthening the seasonal duration of ice-free conditions in the Chukchi Sea.

Acknowledgments
This study was supported by NSF Grants PLR 1603914 and OPP 1748953 (both Serreze) and NSF Arctic Observing Network Grants PLR 1304052 and PLR 1758565 (both Woodgate). The A3 Mooring data are available from the University of Washington, Seattle (http://psc.apl.washington.edu/HLD/Bstrait/Data/BeringStraitMooringDataArchive.html). Data from the MERRA2 reanalysis are available online (at https://gmao.gsfc.nasa.gov/reanalysis/MERRA-2/).

References

Aagaard, K., Roach, A. T., & Schumacher, J. D. (1985). On the wind-driven variability of the flow through Bering Strait. *Journal of Geophysical Research*, *90*(C4), 7213–7221. https://doi.org/10.1029/JC090iC04p07213

Aagaard, K., Weingartner, T. J., Danielson, S. L., Woodgate, R. A., Johnson, G. C., & Whitledge, T. E. (2006). Some controls on flow and salinity in Bering Strait. *Geophysical Research Letters*, *33*, L19602. https://doi.org/10.1029/2006GL026612

Ahlnas, K., & Garrison, G. R. (1985). Satellite and oceanographic observations of the warm coastal current in the Chukchi Sea. *Arctic*, *37*, 244–254.

Clement, J. L., Maslowski, W., Cooper, L. W., Grebmeier, J. M., & Walczowski, W. (2005). Ocean circulation and exchanges through the northern Bering Sea—1979–2001 model results. *Deep Sea Research Part II: Topical Studies in Oceanography*, *52*(24–26), 3509–3540.

Coachman, L. K., & Aagaard, K. (1966). On the water exchange through Bering Strait. *Limnology and Oceanography*, *11*, 44–59. https://doi.org/10.4319/lo.1966.11.1.0044

Danielson, S., Hedstrom, K., Aagaard, K., Weingartner, T. J., & Curchitser, E. (2012). Wind-induced reorganization of the Bering shelf circulation. *Geophysical Research Letters*, *39*, 8601. https://doi.org/10.1029/2012GL051231

Danielson, S., Weingartner, T. J., Aagaard, K., Zhang, J., & Woodgate, R. (2012). Circulation on the central Bering Sea shelf, July 2008 to July 2010. *Journal of Geophysical Research*, *117*, C10003. https://doi.org/10.1029/2012JC008303

Danielson, S., Weingartner, T. J., Hedstrom, K. S., Aagaard, K., Woodgate, R., Curchister, E., & Satebeno, P. J. (2014). Coupled wind-forced controls on the Bering-Chukchi shelf circulation and the Bering Strait throughflow: Ekman transport, continental shelf waves, and variation of the Pacific-Arctic sea surface height gradient. *Progress in Oceanography*, *125*, 40–61. https://doi.org/10.1016/j.pocean.2014.04.006

Fedorova, A. P., & Yankina, A. S. (1963). The passage of Pacific Ocean water through the Bering Strait into the Chukchi Sea, *Deep Sea Res. Oceanogr. Abstr.*, *20*, 217–224.

Gelaro, R., McCarty, W., Suarez, M. J., Todling, R., Molod, A., Takacs, L., et al. (2017). The Modern-Era Retrospective Analysis for Research and Applications, Version 2 (MERERA-2). *Journal of Climate*, *30*(14), 5419–5454. https://doi.org/10.1175/JCLI-D-16-0758.1

Mantua, N. J., Hare, S. R., Zhang, Y., Wallace, J. M., & Francis, R. C. (1997). A Pacific interdecadal climate oscillation with impacts on salmon production. *Bulletin of the American Meteorological Society*, *78*, 1069–1079.

Morris, B. A. (2019). Seasonality and forcing factors of the Alaskan Coastal Current in the Bering Strait from July 2011 to July 2012, Master of Science thesis, University of Washington, 86.

Newman, M., Alexander, M. A., Ault, T. R., Cobb, K. M., Deser, C., Di Lorenzo, E., et al. (2016). The Pacific Decadal Oscillation, revisited. *Journal of Climate*, *29*(12), 4399–4427. http://doi.org/10.1175/JCLI-D-15-0508.1

Ogi, M., & Wallace, J. M. (2007). Summer minimum Arctic sea ice extent and the associated summer atmospheric circulation. *Geophysical Research Letters*, *34*, L12705. https://doi.org/10.1029/2007GL029897

Overland, J. E., Francis, J. A., Hanna, E., & Wang, M. (2012). The recent shift in early summer Arctic atmospheric circulation. *Geophysical Research Letters*, *39*, L19804. https://doi.org/10.1029/2012GL053268

Paquette, R. G., & Bourke, R. H. (1974). Observations on the coastal current of arctic Alaska. *Journal of Marine Research*, *32*, 195–207.

Peralta-Ferriz, C., & Woodgate, R. A. (2017). The dominant role of the East Siberian Sea in driving the oceanic flow through the Bering Strait—Conclusions from GRACE ocean mass satellite data and in-situ mooring observations between 2002 and 2016. *Geophysical Research Letters*, *44*, 11,472–11,481. https://doi.org/10.1002/2017GL075179

Reynolds, R. W., Smith, T. M., Liu, C., Chelton, D. B., Casey, K. S., & Schlax, M. G. (2007). Daily high-resolution-blended analyses for sea surface temperature, *J. Climate*, *20*, 5473–5496.

Roach, A. T., Aagaard, K., Pease, C. H., Salo, S. A., Weingartner, T. J., Pavlov, V., & Kulakov, M. (1995). Direct measurements of transport and water properties through the Bering Strait. *Journal of Geophysical Research*, *100*(C9), 18,443–18,457. https://doi.org/10.1029/95JC01673

Save, H., Bettadpur, S., & Tapley, B. D. (2016). High resolution CSR GRACE RL05 mascons, *J. Geophys. Res. Solid Earth*, *121*, 7547–7569. https://doi.org/10.1002/2016JB013007

Screen, J. A., Simmonds, I., & Keay, K. (2011). Dramatic interannual changes of perennial Arctic sea ice linked to abnormal summer storm activity. *Journal of Geophysical Research*, *116*, D15105. https://doi.org/10.1029/2011JD015847

Serreze, M. C., & Barrett, A. P. (2008). The summer cyclone maximum over the central Arctic Ocean, *J. Climate*, *21*, 1048–1065. https://doi.org/10.1175/2007JCLI1810.1

Serreze, M. C., & Barrett, A. P. (2011). Characteristics of the Beaufort Sea high. *Journal of Climate*, *24*, 159–182. https://doi.org/10.1175/2010JCL3636.1

Serreze, M. C., Crawford, A. D., Stroeve, J. C., Barrett, A. P., & Woodgate, R. A. (2016). Variability, trends, and predictability of seasonal sea ice retreat and advance in the Chukchi Sea. *Journal of Geophysical Research: Oceans*, *121*, 7308–7325. https://doi.org/10.1002/2016JC011977

Serreze, M. C., & Meier, W. N. (2018). The Arctic's sea ice cover: Trends, variability, predictability, and comparisons to the Antarctic. *Annals of the New York Academy of Sciences*, *1436*, 36–53. https://doi.org/10.1111/nyas.13856

Serreze, M. C., Stroeve, J., Barrett, A. P., & Boisvert, L. N. (2016). Summer atmospheric circulation anomalies over the Arctic Ocean and their influences on September sea ice extent: A cautionary tale. *Journal of Geophysical Research: Atmospheres*, *121*, 11,463–11,485. https://doi.org/10.1002/2016JD025161

Spall, M. A. (2007). Circulation and water mass transformation in a model of the Chukchi Sea. *Journal of Geophysical Research*, *112*, C05025. https://doi.org/10.1029/2005jc003364

Steele, M., Morison, J., Ermold, W., Rigor, I., Ortmeyer, M., & Shimada, K. (2004). Circulation of summer Pacific halocline water in the Arctic Ocean. *Journal of Geophysical Research*, *109*, C02027. https://doi.org/10.1029/2003JC002009

Stigebrandt, A. (1984). The North Pacific: A gobal-scale estuary. *Journal of Physical Oceanography*, *14*, 464–470. https://doi.org/10.1175/1520-0485(1984)014<0464:TNPAGS>2.0.CO;2

United States Navy (2014). *The United States Navy Artic Roadmap for 2014 to 2030* (p. 38). Washington, DC: Department of the Navy. www.navy.mil/docs/USN_arctic_roadmap.pdf

Wang, J., Zhang, J., Watanabe, E., Ikeda, M., Mizobata, K., Walsh, J. E., et al. (2009). Is the dipole anomaly a major driver to record lows in Arctic summer sea ice extent? *Geophysical Research Letters*, *36*, L05706. https://doi.org/10.1029/2008GL036706

Woodgate, R. A. (2018). Increases in the Pacific inflow to the Arctic from 1990 to 2015, and insights into seasonal trends and driving mechanisms from year-round Bering Strait mooring data. *Progress in Oceanography*, *160*, 124–154. https://doi.org/10.1016/j.pocean.2017.12.007

Woodgate, R. A., & Aagaard, K. (2005). Revising the Bering Strait freshwater flux into the Arctic Ocean. *Geophysical Research Letters*, *32*, L02602. https://doi.org/10.1029/2004GL021747

Woodgate, R. A., Aagaard, K., & Weingartner, T. J. (2005a). A year in the physical oceanography of the Chukchi Sea: Moored measurements from autumn 1990-1991. *Deep Sea Research Part II: Topical Studies in Oceanography*, *52*(24-26), 3116–3149. https://doi.org/10.1016/j.dsr2.2005.10.016

Woodgate, R. A., Aagaard, K., & Weingartner, T. J. (2005b). Monthly temperature, salinity, and transport variability of the Bering Strait through flow. *Geophysical Research Letters*, *32*, L04601. https://doi.org/10.1029/2004GL021880

Woodgate, R. A., Johnson, J., Peralta-Ferriz, C., Stafford, K., Escajeda, E., Panicker, D., & Irving, B. (2017). *Bering Strait Norseman II 2017 Mooring Cruise Report* (pp. 100). Seattle, WA: University of Washington. (Available at psc.apl.washington.edu/BeringStrait.html.)

Woodgate, R. A., Stafford, K. M., & Prahl, F. G. (2015). A synthesis of year-round Interdisciplinary mooring measurements in the Bering Strait (1990–2014) and the RUSALCA years (2004–2011). *Oceanography*, *28*(3), 46–67. https://doi.org/10.5670/oceanog.2015.57

Woodgate, R. A., Weingartner, T. J., & Lindsay, R. (2010). The 2007 Bering Strait oceanic heat flux and anomalous Arctic sea-ice retreat. *Geophysical Research Letters*, *37*, L01602. https://doi.org/10.1029/2009GL041621

Woodgate, R. A., Weingartner, T. J., & Lindsay, R. (2012). Observed increases in Bering Strait oceanic fluxes from the Pacific to the Arctic from 2001 to 2011 and their impacts on the Arctic Ocean water column. *Geophysical Research Letters*, *39*, L24603. https://doi.org/10.1029/2012GL05409